Sensitivity of a dielectric layered structure on a scale below the periodicity: A fully local homogenized model

Agnès Maurel[1] and Jean-Jacques Marigo[2]
[1]*Institut Langevin, CNRS UMR 7587, ESPCI Paris, PSL Research University, 1 rue Jussieu, 75005, Paris - France*
[2]*Laboratoire de Mécanique du Solide, Ecole Polytechnique, Route de Saclay, Palaiseau 91120, France*

(Received 18 February 2018; revised manuscript received 7 June 2018; published 19 July 2018)

We inspect the unusual scattering properties reported recently for structures alternating dielectric layers of subwavelength thicknesses near the critical angle for total reflection. In TE polarization, the unusual scattering properties are captured by an effective model with an accuracy less than 1% up to $kd \sim 0.1$. It is shown that the propagation is simply dispersive with local dispersion while the boundary layer effects are captured through a nonintuitive transmission condition. The resulting model involves two parameters depending only on the characteristics of the multilayer and which are given in closed forms. Besides, we show that a discrete description of the spectrum using the layer thickness d as unit of measure misses the complexity of the continuous spectrum exhibiting strong variations within the scale d. This ultrasensitivity to variations below d is attributable to strong boundary layer effects and, for large structures, to a cooperation between the boundaries and the phase accumulation within the structure.

DOI: 10.1103/PhysRevB.98.024306

I. INTRODUCTION

Multilayered metamaterials are one-dimensional structures alternating layers with subwavelength thicknesses. Because the periodicity d of the layers is small compared to the incident wavelength $1/k$, the scattering properties of such a multilayered structure are in general well recovered when one replaces the actual structure by a homogeneous analog. The procedure to characterize the equivalent homogeneous medium is the homogenization and at the dominant order, any homogenization procedure yields the prediction of the effective medium approximation (EMA). Although the validity of EMA is *a priori* only restricted to the condition $kd \ll 1$, it was already known that metallodielectric structures alternating layers with negative and positive indices may exhibit scattering properties which are not correctly described by EMA. This was attributable to the rapid variations of the field within the unit cell due to high-index volume modes, and nonlocal theories were proposed [1–3].

In comparison, all-dielectric systems with permittivities of the same order as the surrounding media were believed to be accurately described by the EMA. However, Sheinfux and co-workers have shown recently that dielectric multilayered metamaterials exhibit scattering properties highly sensitive to the thickness and the arrangement of the layers in the vicinity of the critical angle of total reflection [4]; again, the EMA fails to explain this sensitivity. The study in [5] has confirmed and complemented these findings for structures of infinite, semi-infinite, and finite extents. It has been notably shown that (i) for infinite structures, the actual dispersion relation given by Bloch-Floquet analysis obeys the EMA prediction, (ii) the reflectance by semi-infinite structures is insensitive to the arrangement of the layers near the boundary and does not differ much from its homogenized counterpart, and (iii) in contrast, for structures of finite extent, the scattering properties contradict the EMA prediction even for small $kd \sim 0.1$. Since, this high sensitivity has been confirmed experimentally for periodic structures [6] and exploited to produce unusual Anderson localization when introducing disorder in the layer thicknesses [7,8].

From a theoretical point of view, improved models have been proposed. In [3], the expansion of the Bloch-Floquet dispersion relation is performed to get the first correction in $(kd)^2$ to EMA prediction. This correction is sufficient to explain the sensitivity of the structure to the periodicity of the layers but it is unable to explain its sensitivity to the arrangement of the layers at the boundaries or to the materials surrounding the structure. To explain these latter properties, improved models aim to recover boundary effects at the extremities of the structure by enriching the governing equations in the effective problem. Chebykin and co-workers [2,9] used the methodology proposed in [10]; assuming that the structure is excited by an external current results in an additional electric polarization which renders the relation between electric displacement and electric field more involved. While the presented approach allows one to account for local/nonlocal dispersion, it is not clear that the sensitivity of the structure to the layer material ending the structure is captured. In [11], this approach is generalized by including generalized relations between the electric displacement and the magnetic induction vector and the electric and magnetic fields by means of the permittivity and permeability tensors and two gyration pseudotensors. The resulting system is underdetermined, thus it does not permit one to uniquely determine the material parameters; these latter are obtained on the basis of clever physical-based assumptions (see also [12] in the context of hyperbolic metamaterials). In particular, it is shown that, at the first order, the effective gyrotropy is surface induced and cancels when the structure starts with half a layer instead of an entire one, a result that we shall recover in the present study.

At the next order, the effective permittivity and permeability do not reduce to scalars and make nonlocal dispersion appear. Although this result is not expected from the Bloch-Floquet dispersion relation in TE polarization, the model appears to be very accurate to reproduce the scattering properties of actual structures. Eventually, in [13], the authors use the higher-order correction in the effective permittivity and account for the boundary effects by adding heuristically an extra layer whose properties depend on the permittivities of the surrounding media (in addition to the characteristics of the layers).

Among the different approaches of effective media, the homogenization based on two-scale asymptotic analysis is largely used at the dominant first order (hereafter termed HM_1) which corresponds to the EMA. By construction it provides constant effective parameters which depend on the microstructure only. When conducted at higher orders, spatial dispersion appears, also by construction, and depending on the form of the wave equation, we may expect local or nonlocal dispersion [14–16]. What has been less regarded is the homogenization of structures of finite extent (see [17] for multilayered structures). At any order in the homogenization process, an effective wave equation is obtained but effective transmission conditions at the boundaries of the structure can also be derived. These transmission conditions, often nonintuitive, are particularly relevant when ultrathin metamaterial structures are considered, and they have been regarded primarily in this context (see, e.g., [18,19]). In this case, nonlocality is invoked when the transmission conditions involve tangential derivatives of the field.

In the present study, we show that conducting the homogenization up to the third order provides a simple model hereafter termed HM_3 with an effective wave equation involving a permittivity ε_{eff} frequency dependent in agreement with [3,13] and effective transmission conditions involving a parameter $\hat{\varepsilon}$ which depends only on the layer terminating the structure. The modeling is presented in Sec. II where both parameters are given in a closed form; the details of the homogenization procedure are collected in Appendix A. The boundary parameter $\hat{\varepsilon}$ is a key ingredient to accurately describe the scattering properties of the multilayered structure; in particular, it accounts for the intuitive fact that a perfect impedance matching with an output homogeneous medium is in general impossible. This ingredient was introduced heuristically by considering an extra layer at the boundaries of the layered structure in [13]; in [11], it was accounted for through the gyration pseudotensors. In the present model, it is not necessary to introduce *a priori* additional complexities in the model (an extra layer or an effective gyrotropy). The transmission conditions involving $\hat{\varepsilon}$ are deduced from the Helmholtz equation for polarized waves satisfied in the layers and in the input/output media. The breakdown of EMA in the critical conditions is analyzed in the Sec. III. As already pointed out in [4,5], this breakdown is due to a large error of the model for relatively small $kd \sim 0.1$ values but it is not attributable to a failure in the expected convergence of EMA when $kd \to 0$. Conducting the asymptotic analysis at higher order results in an improved model which provides an accuracy better than 1% up to $kd \sim 0.1$ and better than 10% up to $kd \sim 1$. Further results and validations of the model are collected in Sec. IV.

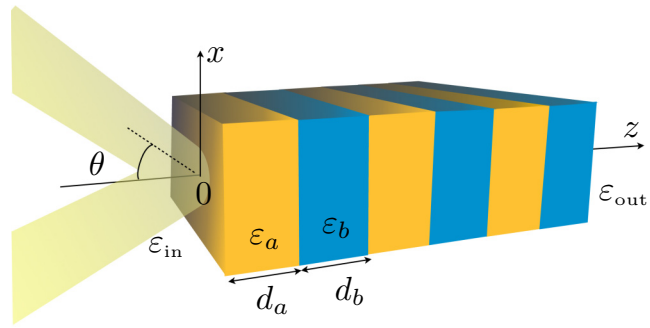

FIG. 1. Multilayer structure illuminated by a plane wave near the critical angle of total reflection ($d = d_a + d_b$ is the period).

In particular, we report a result on the sensitivity of the spectrum in the vicinity of the critical conditions. We show that strong variations of the reflected/transmitted powers occur when the thickness of the first layer is varied continuously from 0 to d. This casts light on the ultrasensitivity of these structures, beyond that already reported within a discrete description of the spectra with d as unit of measure.

II. MODELING

A. The actual and homogenized problems

For an incident wave in the plane (x, z) in TE, the Maxwell equations simplify to the Helmholtz equation applying to the electric field $\mathbf{E} = E(x, z)\boldsymbol{e}_y$, namely, the scalar field E satisfies

$$\Delta E(x, z) + k^2 \varepsilon(z) E(x, z) = 0, \tag{1}$$

with, in the present case, $\varepsilon(z) = \varepsilon_{\text{in}}, \varepsilon_a, \varepsilon_b, \varepsilon_{\text{out}}$, varying along the z axis (Fig. 1). If the incident wave is a plane wave at incidence θ, the problem reduces to a one-dimensional problem along z which can be solved easily, e.g., with the transfer matrix formalism [4]. Our effective model is derived using a two-scale homogenization technique detailed in Appendix A. At the dominant order (order 1), the model HM_1 is that of the classical homogenization and coincides with the EMA. The layered material is replaced by an equivalent homogeneous medium with an effective permittivity

$$\langle \varepsilon \rangle = \frac{d_a \varepsilon_a + d_b \varepsilon_b}{d_a + d_b}. \tag{2}$$

At this order, the transmission conditions at the boundaries of the structure are the usual continuities of the electric field and of its normal derivative. Conducting the analysis at the order 2 leaves us with a model termed HM_2 where the effective medium in the bulk is the same as in EMA, but with modified transmission conditions. The field E is still continuous across the boundary but its normal derivative experiences a jump which is linked to the value of E at the boundary and to a parameter $\hat{\varepsilon}$ depending on the arrangement of the layers terminating the structure ($\hat{\varepsilon}$ does not depend on the characteristics of the surrounding media). Eventually, going up to the order 3 enables the correction in the effective permeability to be obtained. Specifically, our homogenized

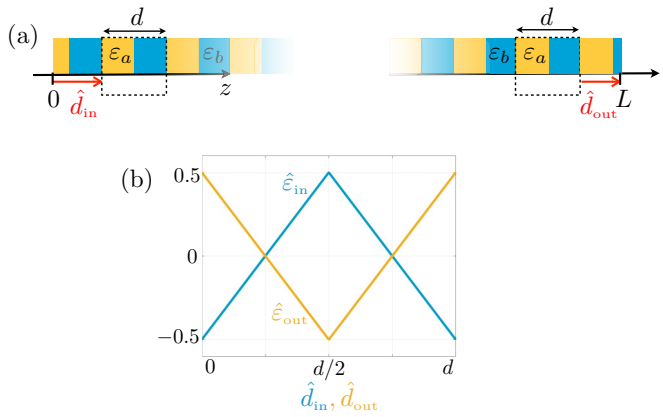

FIG. 2. (a) Convention to characterize the two layers terminating the structure at $z = 0$ and L. (b) Effective parameters $(\hat{\varepsilon}_{\rm in},\ \hat{\varepsilon}_{\rm out})$ from (5), for $\varepsilon_a = 5,\ \varepsilon_b = 1$, and $d_a = d_b = d/2$.

problem HM_3 reads as

$$\begin{aligned} \Delta E + k^2 \varepsilon_{\rm eff}(k) E &= 0, \\ \frac{\partial E}{\partial z}(x,0^+) - \frac{\partial E}{\partial z}(x,0^-) &= k^2 d \hat{\varepsilon}_{\rm in} E(x,0), \\ \frac{\partial E}{\partial z}(x,L^+) - \frac{\partial E}{\partial z}(x,L^-) &= k^2 d \hat{\varepsilon}_{\rm out} E(x,L), \end{aligned} \tag{3}$$

where L is the structure extent. The effective bulk permittivity $\varepsilon_{\rm eff}(k)$ is given by the asymptotic analysis at the order 3. It is the first correction, in $(kd)^2$, of the EMA (see Appendix A 1) and it reads as

$$\varepsilon_{\rm eff}(k) = \langle \varepsilon \rangle + \frac{k^2}{12} \frac{d_a^2 d_b^2}{d^2} (\varepsilon_a - \varepsilon_b)^2, \tag{4}$$

in agreement with the findings of [3] where the correction is obtained from the actual Bloch-Floquet dispersion relation and of [13] where it is derived using approximated expressions of the characteristic matrix (see Appendix A in this reference).

The parameters $\hat{\varepsilon}_{\rm in,out}$ are also obtained explicitly and, as previously said, they depend on the two layers terminating the structure (see Appendix A 2). With the convention shown in Fig. 2, they read as

$$\begin{aligned} \hat{\varepsilon}_{\rm in} &= \frac{(\varepsilon_a - \varepsilon_b)}{d^2} \begin{cases} d_a\left(\hat{d}_{\rm in} - \frac{d_b}{2}\right), & \hat{d}_{\rm in} \in (0, d_b), \\ d_b\left(\frac{d_a}{2} + d_b - \hat{d}_{\rm in}\right), & \hat{d}_{\rm in} \in (d_b, d), \end{cases} \\ \hat{\varepsilon}_{\rm out} &= \frac{(\varepsilon_a - \varepsilon_b)}{d^2} \begin{cases} d_b\left(\frac{d_a}{2} - \hat{d}_{\rm out}\right), & \hat{d}_{\rm out} \in (0, d_a), \\ d_a\left(\hat{d}_{\rm out} - d_a - \frac{d_b}{2}\right), & \hat{d}_{\rm out} \in (d_a, d). \end{cases} \end{aligned} \tag{5}$$

Simple remarks on $\hat{\varepsilon}$ can be drawn as follows:

(1) For a structure containing an integer number N of layers $(L = Nd)$ we have $\hat{d}_{\rm in} = \hat{d}_{\rm out}$, hence $\hat{\varepsilon}_{\rm in} = -\hat{\varepsilon}_{\rm out}$.

(2) A structure starting with a half-layer of material b $(\hat{d}_{\rm in} = d/4)$ or of material a $(\hat{d}_{\rm in} = 3d/4)$ is assigned to the usual conditions of continuity of the E and its normal derivative, at $z = 0$, since $\hat{\varepsilon}_{\rm in} = 0$ in (3). The same applies at $z = L$ with $\hat{\varepsilon}_{\rm out} = 0$ for $\hat{d}_{\rm out} = d/4$ or $\hat{d}_{\rm out} = 3d/4$. This conforms with the prediction given by the surface-induced effective gyrotropy in [11].

(3) Reversely, a structure starting with a complete layer of material a $(\hat{d}_{\rm in} = 0)$ or of material b $(\hat{d}_{\rm in} = d/2)$ realizes extrema $\hat{\varepsilon}_{\rm in} = \pm(\varepsilon_a - \varepsilon_b)\frac{d_a d_b}{2d^2}$.

It is worth noting that the configuration considered in [4,13] corresponds to $\hat{d}_{\rm in} = \hat{d}_{\rm out} = 0$. Thus, $\hat{\varepsilon}_{\rm in} = -\hat{\varepsilon}_{\rm out}$ take maximum values.

The homogenized problems HM_3 correspond to that of a slab filled with a homogeneous material $(\varepsilon_{\rm eff})$ sandwiched between two homogeneous media. Setting $d = 0$ in (3) reduces the model to EMA. Setting $\varepsilon_{\rm eff} = \langle \varepsilon \rangle$ while keeping the transmission conditions in (3) corresponds to HM_2. The order of the models corresponds to their expected convergences, in (kd) for EMA and in $(kd)^2$ for HM_2. Eventually, HM_3 is a hybrid model, with a convergence in $(kd)^2$ (see Appendix A). At any order, the effective structure has local properties in its bulk with $\varepsilon_{\rm eff}$ depending on the wave number only. The effective transmission conditions are local as well since they involve the field E and its normal derivative in a Robin-like relation (enlightening discussions on nonlocality and effective properties can be found in [20,21]). These local properties are obtained in the polarization TE that we consider in the present study and they would be lost in TM polarization.

B. Scattering properties of the homogenized structure

1. *Semi-infinite structure—Local scattering coefficients*

The scattering properties of the slab of extent L can be deduced from that at the single interfaces, at $z = 0$ and L. These latter are obtained considering the solution of the whole problem with incident waves coming from $z = \pm\infty$, specifically

$$E = e^{i\gamma x} \begin{cases} a^+ e^{i\alpha_{\rm in} z} + a^- e^{-i\alpha_{\rm in} z}, & z \in (-\infty, 0) \\ b^+ e^{i\alpha z} + b^- e^{-i\alpha z} & z \in (0, L) \\ c^+ e^{i\alpha_{\rm out}(z-L)} + c^- e^{-i\alpha_{\rm out}(z-L)} & z \in (L, \infty), \end{cases}$$

with γ the wave number along x and $(\alpha_{\rm in}, \alpha, \alpha_{\rm out})$ those along z defined by

$$\begin{aligned} \gamma &= k\sqrt{\varepsilon_{\rm in}} \sin\theta, \quad \alpha_{\rm in} = k\sqrt{\varepsilon_{\rm in}} \cos\theta, \\ \alpha &= \sqrt{k^2 \varepsilon_{\rm eff} - \gamma^2}, \quad \alpha_{\rm out} = \sqrt{k^2 \varepsilon_{\rm out} - \gamma^2}. \end{aligned} \tag{6}$$

We get the local scattering coefficients, accounting for the transmission conditions (3) at $z = 0, L$, of the form

$$\begin{aligned} r_{\rm in}^+ &= -\frac{\alpha - \overline{z_{\rm in}}}{\alpha + z_{\rm in}}, \quad t_{\rm in}^+ = \frac{2\alpha_{\rm in}}{\alpha + z_{\rm in}}, \\ r_{\rm in}^- &= \frac{\alpha - z_{\rm in}}{\alpha + z_{\rm in}}, \quad t_{\rm in}^- = \frac{2\alpha}{\alpha + z_{\rm in}}, \\ r_{\rm out}^+ &= \frac{\alpha - z_{\rm out}}{\alpha + z_{\rm out}}, \quad t_{\rm out}^+ = \frac{2\alpha}{\alpha + z_{\rm out}}, \\ r_{\rm out}^- &= -\frac{\alpha - \overline{z_{\rm out}}}{\alpha + z_{\rm out}}, \quad t_{\rm out}^- = \frac{2\alpha_{\rm out}}{\alpha + z_{\rm out}}, \\ \text{with} \quad z_{\rm in} &= \alpha_{\rm in} + i\hat{\varepsilon}_{\rm in} k^2 d, \quad z_{\rm out} = \alpha_{\rm out} + i\hat{\varepsilon}_{\rm out} k^2 d, \end{aligned} \tag{7}$$

where we have defined at the input interface $a^- = r_{\rm in}^+ a^+ + t_{\rm in}^- b^-$, $b^+ = t_{\rm in}^+ a^+ + r_{\rm in}^- b^-$ and at the output interface $b^- e^{-i\alpha L} = r_{\rm out}^+ b^+ e^{i\alpha L} + t_{\rm out}^- c^-$, $c^+ = t_{\rm out}^+ e^{i\alpha L} b^+ + r_{\rm out}^- c^-$.

In [5], the reflectance $\mathcal{P}_r = |r_{\rm in}^+|^2$ of semi-infinite structures is considered. Specifically, the following quantities are

considered: (i) $\Delta\mathcal{P}_{\mathrm{r},d} = |r_{\mathrm{in}}^{+}|^2_{(kd)} - |r_{\mathrm{in}}^{+}|^2_{(kd)_0}$ measures the sensitivity of the reflectance on the layer thickness d, with $(kd)_0 \sim 5\times10^{-3}$ representing $kd \to 0$ and $(kd) \sim 0.1$, and (ii) $\Delta\mathcal{P}_{\mathrm{r},o} = |r_{\mathrm{in}}^{+}|^2_{a} - |r_{\mathrm{in}}^{+}|^2_{b}$ measures the difference in the reflectance of a structure starting with a layer of material a with that of a structure starting with a layer of material b. Those quantities are considered near the critical angle of total reflection

$$\theta_{\mathrm{c}} = \arcsin\sqrt{\frac{\langle\varepsilon\rangle}{\varepsilon_{\mathrm{in}}}}. \tag{8}$$

From (7), we have

$$|r_{\mathrm{in}}^{+}|^2 \simeq 1 - kd\,\frac{d_a d_b\,|\varepsilon_a-\varepsilon_b|}{\sqrt{3\varepsilon_{\mathrm{in}}}\,d^2\cos\theta_{\mathrm{c}}} + O[(kd)^2], \tag{9}$$

which leaves us with

$$\Delta\mathcal{P}_{\mathrm{r},d} \sim -kd\,\frac{d_a d_b\,|\varepsilon_a-\varepsilon_b|}{\sqrt{3\varepsilon_{\mathrm{in}}}\,d^2\cos\theta_{\mathrm{c}}}, \quad \Delta\mathcal{P}_{\mathrm{r},o} = O[(kd)^2]. \tag{10}$$

The above estimates are in agreement with the findings reported in [5]: $\Delta\mathcal{P}_{\mathrm{r},d}$ has the same order of magnitude as kd and is the same whenever the structure starts with a layer of material a or a layer of material b; as a consequence, the reflectances of structures starting with a layer a or with a layer b do not differ significantly with $\Delta\mathcal{P}_{\mathrm{r},o}$ vanishing up to $(kd)^2$.

2. *Reflection and transmission of a structure of finite extent*

The scattering coefficients (R,T) of a structure of finite extent simply follow from the preceding section. Looking for a solution to the scattering problem for a right-going incident wave of amplitude unity of the form

$$E(x,z) = e^{i\gamma x}\begin{cases} e^{i\alpha_{\mathrm{in}}z} + Re^{-i\alpha_{\mathrm{in}}z}, & z\in(-\infty,0)\\ Ae^{i\alpha z} + Be^{-i\alpha(z-L)}, & z\in(0,L)\\ Te^{i\alpha_{\mathrm{out}}(z-L)}, & z\in(L,+\infty),\end{cases}$$

(R,T) are given by

$$R = \frac{r_{\mathrm{in}}^{+}\,e^{-i\alpha L} + \left(t_{\mathrm{in}}^{+}t_{\mathrm{in}}^{-} - r_{\mathrm{in}}^{+}r_{\mathrm{in}}^{-}\right)r_{\mathrm{out}}^{+}\,e^{i\alpha L}}{e^{-i\alpha L} - r_{\mathrm{out}}^{+}r_{\mathrm{in}}^{-}\,e^{i\alpha L}},$$

$$T = \frac{t_{\mathrm{in}}^{+}t_{\mathrm{out}}^{+}}{e^{-i\alpha L} - r_{\mathrm{out}}^{+}r_{\mathrm{in}}^{-}\,e^{i\alpha L}}. \tag{11}$$

Expectedly, the bulk effective permittivity $\varepsilon_{\mathrm{eff}}$ and the interface effective permittivities $(\hat\varepsilon_{\mathrm{in}},\hat\varepsilon_{\mathrm{out}})$ do not play the same role: while $\varepsilon_{\mathrm{eff}}$ affects the phase accumulation during wave propagation through $e^{i\alpha L}$, $\hat\varepsilon_{\mathrm{in}}$ and $\hat\varepsilon_{\mathrm{out}}$ affect the local scattering coefficients at the interfaces at $z=0$ and L, respectively.

In general, the corrections in (kd) due to $(\hat\varepsilon_{\mathrm{in}},\hat\varepsilon_{\mathrm{out}})$ and that in $(kd)^2$ due to $\varepsilon_{\mathrm{eff}}$ are small and the scattering is that of a usual slab behaving as a Fabry-Perot interferometer. However, near the critical angle θ_{c}, the wave number α goes from real to imaginary in an intricate way. Indeed, denoting $\delta\varepsilon_k = \varepsilon_{\mathrm{eff}} - \langle\varepsilon\rangle \propto (kd)^2$ the shift in the permittivity from (4) and $\delta\varepsilon_\theta = \varepsilon_{\mathrm{in}}\sin^2\theta - \langle\varepsilon\rangle$ the shift in the incidence, the pattern of $\alpha = k\sqrt{\delta\varepsilon_k - \delta\varepsilon_\theta}$ in the (k,θ) space is already quite involved. The situation becomes even more involved when the output medium is almost matched to the slab with $\varepsilon_{\mathrm{out}} = \langle\varepsilon\rangle + \delta\varepsilon_{\mathrm{out}}$; then, $z_{\mathrm{out}} = k(\sqrt{\delta\varepsilon_{\mathrm{out}} - \delta\varepsilon_\theta} + ikd\hat\varepsilon_{\mathrm{out}})$ has also a (k,θ) dependence. It results that the scattering coefficients $(r_{\mathrm{out}}^{+}, t_{\mathrm{out}}^{+})$ at the output interface [see (7)] involve a combination of small and (k,θ)-dependent terms, which allows us to anticipate a complex shape of the spectrum. In particular, even for a given output medium, it is impossible to provide approximate expressions of $(r_{\mathrm{out}}^{+}, t_{\mathrm{out}}^{+})$ valid for any (k,θ).

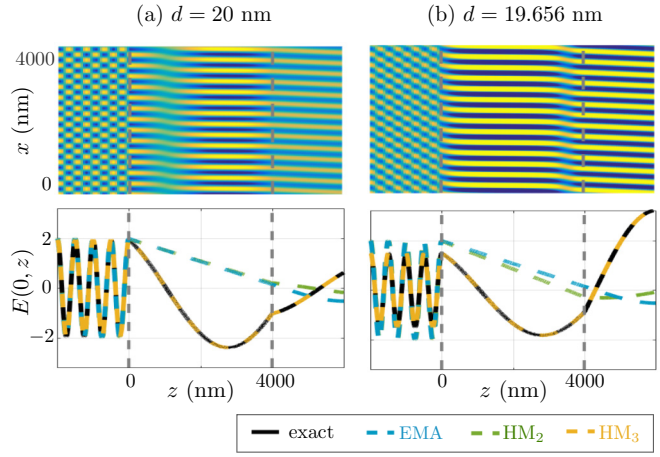

FIG. 3. Fields $E(x,z)$ and profiles $E(0,z)$ for an incident wave ($\theta = 60^\circ$, $\varepsilon_{\mathrm{out}} = \varepsilon_{\mathrm{eff}}$) on multilayers of same extent $L = 4000$ nm with two layer thicknesses which differ by less than 2% (in both cases $d_a = d_b = d/2$). (a) $|R|^2 = 91\%$ and (b) $|R|^2 = 25\%$.

Eventually, note that the scattering coefficients (R,T) in (11) are valid except if $\alpha = 0$ [$\theta = \arcsin\sqrt{\varepsilon_{\mathrm{eff}}(k)/\varepsilon_{\mathrm{in}}}$]; in this case, the solution for $z>0$ has to be sought with a linear dependence in z. As this situation corresponds to a single point in the (k,θ) spectrum, it is disregarded in the present study.

III. CONVERGENCE/ACCURACY OF THE HOMOGENIZED MODELS

We consider the same parameters as in [4]: $k = 2\pi/(500\text{ nm})$, $\varepsilon_{\mathrm{in}} = 4$, $\varepsilon_a = 5$, $\varepsilon_b = 1$, and $d = 20$ nm with $d_a = d_b = d/2$. We shall consider the critical conditions, namely, in the vicinity of $\varepsilon_{\mathrm{out}} \simeq \langle\varepsilon\rangle = 3$ and $\theta \simeq \theta_{\mathrm{c}} = 60^\circ$. Note that $\varepsilon_{\mathrm{eff}} = 3.053$ and $\arcsin\sqrt{\varepsilon_{\mathrm{eff}}(k)/\varepsilon_{\mathrm{in}}} = 60.09^\circ$ at this frequency. Following [4], we term regular (respectively, reverse) order configuration that of a structure with $L = Nd$, N integer, starting with an entire layer of material a (respectively, material b).

A. A typical example

To begin with, we report in Fig. 3 the fields $E(x,z)$ calculated numerically for two structures of same extent $L = 4000$ nm and a small change in d, from $d = 20$ nm (regular order with $L = 200d$) to $d = 19.656$ nm. The scattering properties of these structures which differ by a relative change in d less than 2% are unexpectedly different, from a quasiperfect reflection to a quasiperfect transmission. Obviously, EMA predicts erroneously the same properties for (a) and (b). Next, because we kept at the entrance an entire layer of material a, only $\hat\varepsilon_{\mathrm{out}}$ is changed in the effective problems HM$_2$ and HM$_3$. With $\hat\varepsilon_{\mathrm{out}} = 0.5$ for the regular order $L = 200d$ (a) and $\hat\varepsilon_{\mathrm{out}} = -0.5$ since $L = 203.5d$ for (b), HM$_2$ detects a difference but fails in predicting the right wave number α within the structure, resulting in a large error. Eventually HM$_3$ captures both effects accurately.

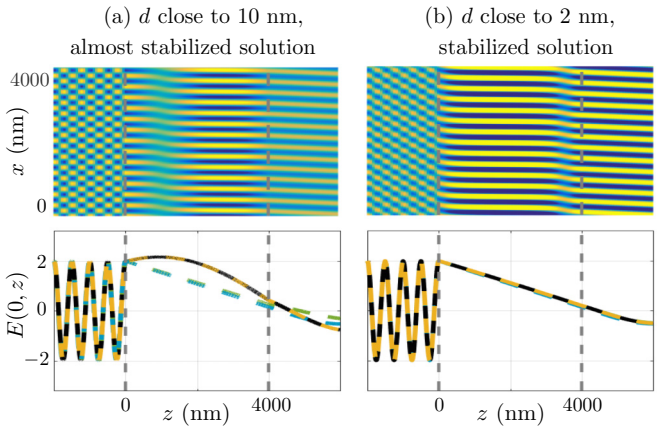

FIG. 4. Same representation as in Fig. 3. (a) The almost stabilized solution, with variations of 5% for variations in d of 2% around $d =$ 10 nm ($|R|^2 \simeq 95\%$). (b) The stabilized solution, with variations of 0.1% for variations in d of 2% around $d = 2$ nm ($|R|^2 = 98\%$).

Now we keep the same extent L but we consider smaller layer thicknesses, with $d = 10$ nm and $d = 9.828$ nm. In this case, the variation of 2% in the thickness does not much affect the scattering properties of the structure, with a variation of only 5%. The field for $d = 10$ nm reported in Fig. 4(a) is undistinguishable from that for $d = 9.828$ nm (not reported). For this almost stabilized solution, the predictions of EMA and HM_2 remain not very accurate when compared to that of HM_3. Eventually, for d of the order of 2 nm, the solution is fully stabilized, with a variation in thickness of 2% producing a variation in the scattering properties of 0.1% [Fig. 4(b)]. In this case, EMA and $HM_{2,3}$ have roughly the same good accuracy.

This example illustrates the fact that the EMA prediction does not fail altogether but rather lacks in robustness when kd increases above $kd = 0.1$, a fact already pointed out in [4]. Below, we further inspect this lack of robustness considering the convergence of the homogenized models.

B. Convergence/accuracy of the models

When conducting an asymptotic analysis, it is assumed that the solution can be expanded in power of the small parameter kd [see, e.g., our expansions in (A2)]. The leading order for $kd = 0$ has to be dominant; afterward, higher order terms in the expansion can be accounted for to provide more accurate predictions for nonzero kd. In particular, the convergence of the leading order prediction when compared to the actual solution is expected in kd; if the leading order fails in this convergence, the whole analysis breaks down altogether and it is useless to conduct the analysis at higher orders. Thus, it makes sense to check that EMA follows the convergence expected in the asymptotic analysis.

Figure 5(a) reports the variations of the transmission

$$\mathcal{P}_T = \text{real}\left(\frac{\alpha_{\text{out}}}{\alpha_{\text{in}}}|T|^2\right) \tag{12}$$

against θ and kd ($\varepsilon_{\text{out}} = \varepsilon_{\text{eff}}$, regular order with $L = 2000$ nm). With $kd \in (10^{-2}, 1)$, we inspect the very low frequency regime up to the borderline case $kd = 1$. Figure 5(b) shows the corresponding errors in the models at the orders 1–3, $|\Delta T/T|$

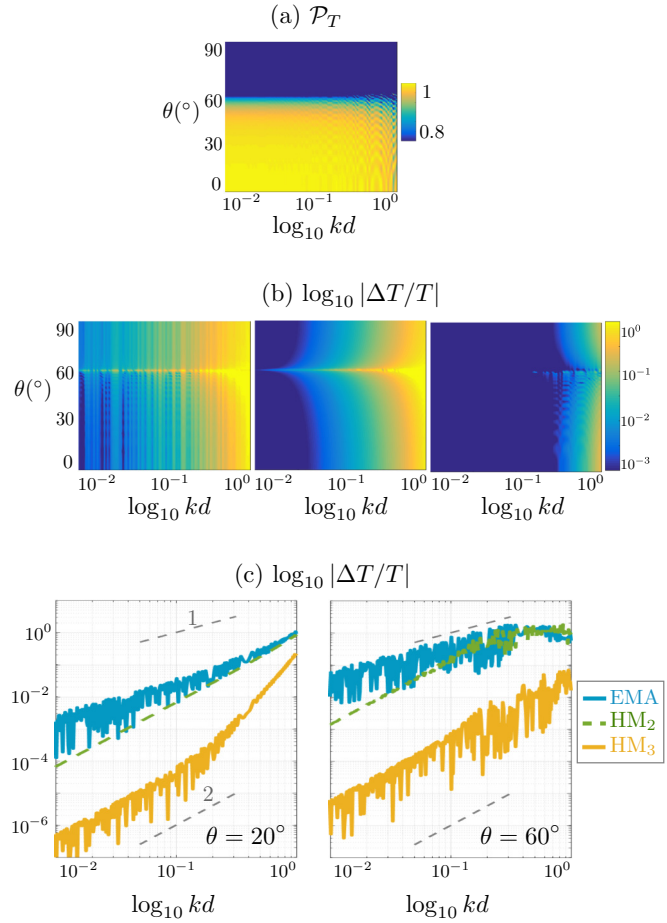

FIG. 5. Convergence of the models. (a) Transmission spectrum. (b) Errors of the models (EMA, HM_2, and HM_3 from the left to the right). (c) Error profiles for $\theta = 20^\circ$ and 60°; dashed gray lines show the slopes 1 and 2.

($\Delta T = T - T_e$) with the reference solution T_e calculated numerically. The EMA error presents scars corresponding to phase mismatches at the boundaries which are removed with HM_2. In comparison, HM_3 significantly reduces the error by about two orders of magnitude.

Eventually, we report in (c) the profiles of the errors for $\theta =$ 20° and 60°. The convergences observed are those expected from the asymptotic analysis: the EMA error increases as (kd) and the HM_2 error as $(kd)^2$. Next our HM_3 model is hybrid and fails in the $(kd)^3$ convergence, being penalized by the correction truncated at the order 2 in the transmission conditions (see Appendix A 2); as such its error increases as $(kd)^2$. It turns out that HM_2 does not significantly improve the accuracy of EMA while HM_3 does. More importantly, at the critical angle $\theta = \theta_c$, the errors in EMA and in HM_2 become significant as soon as $kd = 10^{-2}$ (about 10%) and overcomes 100% for $kd = 0.1$. In comparison, HM_3 has an accuracy of 0.1% up to $kd = 0.1$ and does not exceed 10% up to $kd = 1$. While the running case with $k = 2\pi/(500\text{ nm})$ corresponds to $kd \simeq 0.25$ where the error is very low, it has been stressed in [4] that structures with $d \sim \lambda/10$, hence $kd \sim 0.6$ tends to unity, could be interesting from an applications-oriented perspective since they should be less sensitive to disorder and loss. This

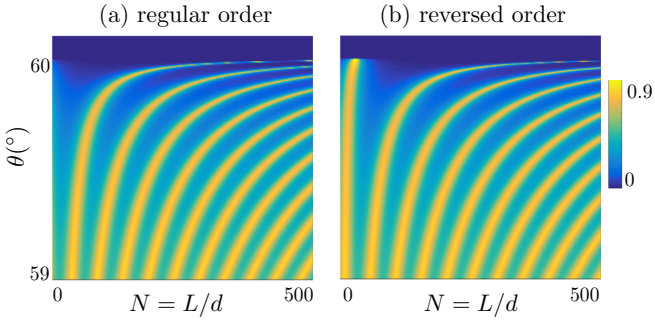

FIG. 6. Discrete transmission spectra; $L = Nd$ varies with d increment.

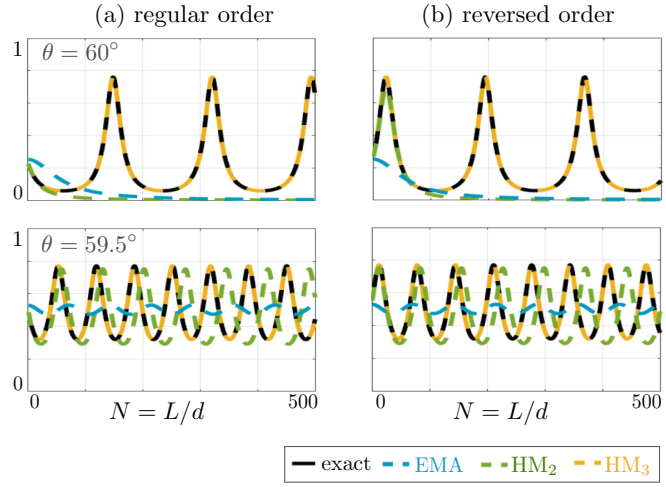

FIG. 7. Transmission against N (integers) at $\theta = 60°$ and 59.5°, from the discrete transmission spectra in Fig. 6.

intermediate regime is clearly a limiting case of the asymptotic analysis which assumes small values of kd; it is commented further in Appendix B. From what has been seen, the hierarchy expected in the homogenized models is verified, which fully justifies their use. In the critical conditions and for $kd > 0.1$, both the boundary layer effects and the correction of α in the bulk have to be accounted for, hence only HM_3 has a low error.

IV. COMPLEXITY OF THE SPECTRUM WITHIN DISCRETE/CONTINUOUS VARIATIONS OF THE STRUCTURE EXTENT

Many illustrations of the EMA failure have been given in the initial paper of Sheinfux and co-workers [4] and later on in [5,11,13]. Most of the reported features concern structures made of an integer number of layers, which is within a discrete description of the problem. However, it was already reported in [4] that the transmission is very sensitive to the length of the terminating layer, hence to a variation smaller than d. This suggests that going toward a continuous description of the problem can be of interest.

In this section, we start by reporting illustrations of the sensitivity of the spectrum within the usual discrete description. Next, we move to its continuous counterpart, which reveals a much stronger complexity.

A. A version of the spectrum with d increment

We consider the spectrum produced by structures of increasing extent $L = Nd$, with N integer. Figure 6 shows the transmission spectra for structures with the regular order (succession a–b at the entrance) and with the reverse order (succession b–a at the entrance); in both cases, the first layer is complete of thickness d. Each spectrum resembles the classical spectrum of a homogeneous slab; however, the regular or reversed order cases are different, exchanging the locations of their maximum transmissions and reflections. This unusual feature already pointed out in [4] is attributable to the boundary layer effects at both extremities, with $\hat{\varepsilon}_{in} = -\hat{\varepsilon}_{out} = -0.5$ for the regular order and $\hat{\varepsilon}_{in} = -\hat{\varepsilon}_{out} = 0.5$ for the reversed one. Note that the same spectra would be obtained in the regular and reversed orders for structures starting with a half-layer of material a or b (thus $\varepsilon_{in,out} = 0$).

Obviously, the EMA fails in predicting these transmission properties (see Fig. 7). The critical angle is underestimated ($\theta = 60°$ in Fig. 7), and below the critical angle, the periodicity $1/\alpha$ of $\mathcal{P}_T$ is overestimated. Capturing the boundary layer effects in HM_2 is the first necessary improvement and it is sufficient for small structures, say αL up to few unities [here for N up to $1/(\alpha d) \sim 55$]. Eventually, HM_3 recovering in addition the correct, small, α value corrects the two drawbacks with an accuracy of 0.2% in the reported case.

To better understand the difference in the spectra for the regular and reversed orders, a continuous variation of the terminating layer is considered. In [4] this was done by increasing the thickness of the terminating layer resulting in changes from $L = Nd$ to $L = (N + 1)d$ [see Fig. 3(b) in this reference]. Here we keep $L = Nd$, with N integer, and we shift of $\delta \in (0, d)$ all the layers within the structure; the direct order $\delta = 0$ and reverse order $\delta = d/2$ are now borderline cases. Doing so, we modify the boundary layer effects only, the effective permittivity in the bulk remaining identical. Besides, since L is a multiple of d, we simply have $\hat{\varepsilon}_{in} = -\hat{\varepsilon}_{out}$ and we shall see that this is not incidental. The resulting variations in the transmission $\mathcal{P}_T$ against δ and N are reported in Fig. 8. The transmission $\mathcal{P}_T$ varies significantly from almost 0 to about 0.8, with extrema reached at $\delta = 0$ and $d/2$ which correspond to the strongest boundary layer effects. Next the pattern of the transmission is periodically repeated along N, with a periodicity dictated by αNd, in the present case for $N \sim 172$. The accuracy of HM_3 to reproduce this pattern is illustrated by splitting the plot and by reporting the numerical solution for $\delta/d > 0.5$ and the HM_3 prediction $\delta < 0.5$; the discrepancy between both is less than 0.5%.

B. Continuous variation of L—A complex cooperation between the bulk and the boundaries

We shall now see that the patterns observed in Figs. 6 and 8 are deeply modified when the increment ΔL in L is decreased; up to now we had $\Delta L = d$. We start with the spectrum of Fig. 8 where the layers were shifted within a structure of extent L. Figure 9(a) reproduces the pattern of Fig. 8 over roughly a period $L/d \in (0, 175)$ and $\Delta L = d$. Next, we decrease the increment to $\Delta L = d/2$, $d/4$ and to a continuous version. We define this continuous version for $\Delta L \lesssim d/40$ producing a

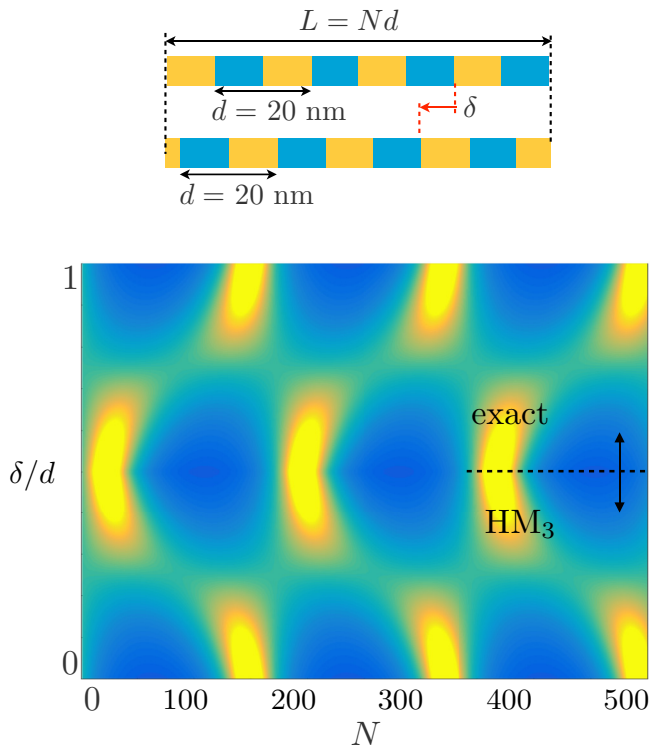

FIG. 8. Variations in the transmission against integers $N = L/d$ and δ/d for $\theta = 60°$; each vertical line corresponds to increasing shifts of the layers within a structure of extent L; $\delta = 0$ is the regular order. The plot reports the numerical calculation for $\delta/d > 0.5$ and the HM_3 prediction for $\delta/d < 0.5$ (the overall discrepancy is of 0.4%).

spectrum which differs by less than 5% from its interpolated version with a step $2\Delta L$; this means that further decreasing

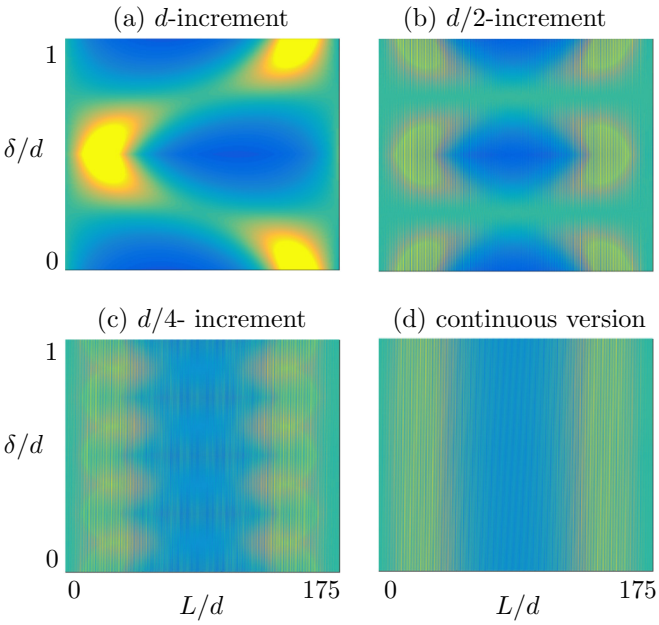

FIG. 9. Spectrum patterns for decreasing pixelization ΔL below d. The pattern (a) is a zoom of Fig. 8 in a period $L/d \in (0175)$; $\theta = 60°$, $\delta = 0$ corresponds to the regular order.

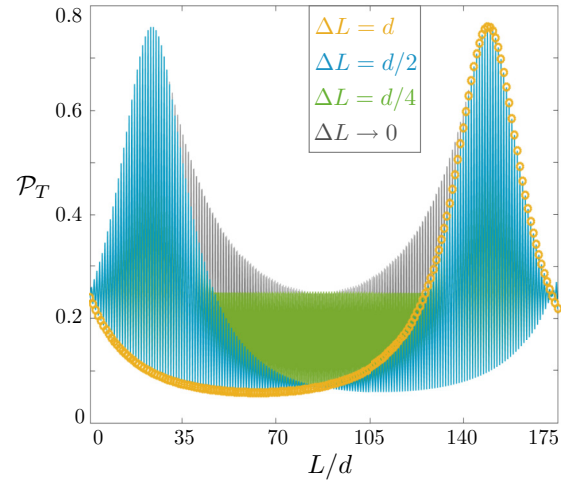

FIG. 10. Profiles of the transmission against L for $\delta = 0$, from Fig. 9; $\Delta L \to 0$ means equal $d/40$ (continuous version).

ΔL does not produce a significant change in the spectrum. The resulting patterns in Figs. 9(a)–9(d) strongly differ revealing a high sensitivity to these different pixelizations. Of course, the vertical lines for L/d integer are conserved from (a) to (d); however, strong fluctuations of the transmission occur in between them. For instance, the region around $\delta = d/2$ and $L/d > 100$ with low transmission in (a) reveals strong local maxima in (b)–(d).

To understand this behavior, let us comment on the variations of $(\hat{\varepsilon}_{\text{in}}, \hat{\varepsilon}_{\text{out}})$ in the plane (L, δ). By construction, $\hat{d}_{\text{in}} = (d - \delta)$ produces $\hat{\varepsilon}_{\text{in}}(\delta)$ independent of L. Next, with $L = Nd + d'$ and $d' \in (0, d)$, we have $\hat{d}_{\text{out}} = \delta + d'$ for $\delta \in (0, d - d')$ and $\hat{d}_{\text{out}} = \delta + d' - d$ for $\delta \in (d - d', d)$ (note that the variations of $\hat{d}_{\text{in}}$ and $\hat{d}_{\text{out}}$ would be even more involved for $d_a \neq d_b$). It results that $\hat{\varepsilon}_{\text{out}}$ against L is d periodic but for, e.g., $L = d$, it varies with δ according to $\hat{\varepsilon}_{\text{out}} = -\hat{\varepsilon}_{\text{in}}$, the regular order. Hence, the pattern of $\hat{\varepsilon}_{\text{out}}$ is composed of inclined layers in the (L, δ) plane. Among the couples $(\hat{\varepsilon}_{\text{in}}, \hat{\varepsilon}_{\text{out}})$, an increment $\Delta L = d$ selects those with $\hat{\varepsilon}_{\text{out}} = -\hat{\varepsilon}_{\text{in}}$ and as such it misses the infinity of other combinations. By decreasing ΔL we get more and more back which complement the spectrum. This is further illustrated in Fig. 10 where we report the profiles of $\mathcal{P}_T$ against L for decreasing increments. The various couples $(\hat{\varepsilon}_{\text{in}}, \hat{\varepsilon}_{\text{out}})$ varying within d produce strong variations of the scattering, beyond the apparent relative simplicity of the d-increment version. Note that our model HM_3 reproduces the continuous version of the spectrum in Figs. 9 and 10 with a discrepancy less than 1%. It is worth noting that in the present case, for $kd \sim 0.25$ the HM_3 prediction remains very accurate for large N values; additional results in the intermediate regime $kd \sim 1$ are reported in Appendix B which reveals an increase in the error for increasing L/d value, in addition to the expected increasing error for increasing kd.

Now, we consider the spectrum reported in Fig. 6 for d-incremented extent of the structure, and we move to its continuous version. We focus on a tiny region of Fig. 6 corresponding to $L/d \in (490, 500)$ and small variations of the angle near the critical angle. The result is shown in Fig. 11: in (a) a zoom of Fig. 6 with $\Delta L = d$ and in (b) its continuous version with $\Delta L = d/50$. The difference between both patterns is

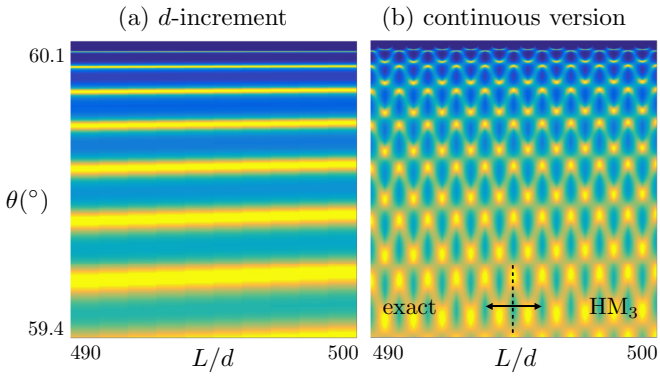

FIG. 11. Modification of the spectrum pattern for (a) the discrete version of the spectrum $\Delta L = d$ and (b) for its continuous counterpart, $\Delta L = d/50$; same representation as in Fig. 6 for the regular order. In (b), the numerical solution is reported for $L/d < 495$ and the HM_3 prediction is reported for $L/d > 495$.

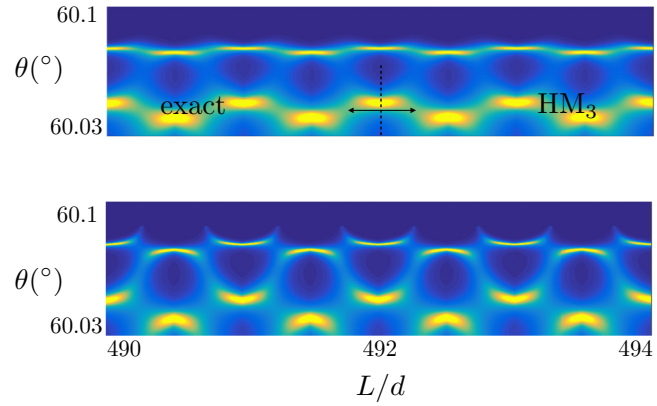

FIG. 12. Details of the transmission patterns near the critical angle for $\varepsilon_{out} = 3.001$ (top panel) and $\varepsilon_{out} = \varepsilon_{eff} = 3.053$ (bottom panel).

again impressive but amusingly, the tiny pixelization reveals now a nice complex structuration due to strong fluctuations in the transmission within the scale d. Here, the variations of $(\hat{\varepsilon}_{in}, \hat{\varepsilon}_{out})$ are simpler than previously. As L increases while keeping the regular order at $z = 0$, $\hat{\varepsilon}_{in} = -0.5$ is constant and $\hat{\varepsilon}_{out}$ varies continuously with L being otherwise independent of θ.

For these large extents, the observed pattern results from cooperation between the bulk of the structure and its boundaries. On the one hand, interferences of the Fabry-Perot type take place, being dictated by the variations of αL. Several maxima in transmission are visible within a small range in θ just below θ_c' realizing $\sin^2\theta_c' \simeq \varepsilon_{eff}/\varepsilon_{in}$; with α in (6), a fuzzy estimation gives $\theta \sim \theta_c' - (n\pi/kL)^2$ which are nearly constant angles with a small increase in L, as captured in (a); the same shape would be obtained for ε_{out} far from ε_{eff}. On the other hand, varying $\hat{\varepsilon}_{out}$ affects the values of θ realizing these maxima. For ε_{out} far from ε_{eff}, these changes are incidental; for ε_{out} close to ε_{eff}, they are sufficient to structure the spectrum below the size d. This effect is further illustrated in Appendix C where we report results on the influence of the layer thickness.

Eventually, the spectrum is also very sensitive to ε_{out} in the vicinity of ε_{eff}; this is illustrated in Fig. 12 where we report the patterns for $\varepsilon_{out} = 3.001$ and $\varepsilon_{out} = \varepsilon_{eff} = 3.053$. In the vicinity of the critical conditions, the scattering properties become sensitive to any small change in the wave incidence and in the length of the structure, but also in a small change in the permittivity of the output medium.

V. CONCLUSIONS

In this study, we have presented a model based on homogenization of finite extent structure and whose high accuracy has been exemplified; the model is fully local, both in the wave equation and the transmission conditions, of the Robin's type. It involves a permittivity ε_{eff} in the bulk of the effective material and two effective boundary parameters $(\hat{\varepsilon}_{in}, \hat{\varepsilon}_{out})$. In the present case, the bulk parameter ε_{eff} in (4) contains a correction in $(kd)^2$ already derived in [3,13]. The boundary parameters $(\hat{\varepsilon}_{in}, \hat{\varepsilon}_{out})$ in (5) enter in unusual transmission conditions which are corrections in (kd) of the usual continuity conditions; they do not depend on the surrounding materials, which is an exception rather than the rule, but only on the arrangement of the layers at the structure boundaries. These boundary layer effects are the key point to explain the unusual scattering properties of multilayered metamaterials. Eventually, guided by our model, we have exemplified the extreme sensitivity of the spectra at a scale smaller than d well beyond the sensitivity usually reported using a discretization of L with d as unit of measure. It is worth noting that the high accuracy of the presented model allows us to capture these strong variations.

Extensions of the present work include the case of TM polarization for which nonlocality is expected, and layers alternating negative and positive index materials, as for metal-dielectric multilayered metamaterial. It would also be interesting to see if recent approaches based on homogenization for so-called quasiperiodic [22] or locally periodic [23] systems can be applied to periodic structures in the presence of disorder to explain the recent results of [8] on the interplay between evanescent waves and Anderson localization.

ACKNOWLEDGMENTS

A.M. thanks V. Pagneux for fruitful discussions. The authors acknowledge the financial support of the CNRS-MI through Grant PomS/Defi Infinity.

APPENDIX A: HIGH-ORDER HOMOGENIZATION

In this Appendix we detail the asymptotic analysis which provides the homogenized models $HM_{1,2,3}$. The model HM_1 coincides with the EMA; the model used in our analysis is HM_3, corresponding to Eqs. (3). A similar derivation can be found in [17] (up to the second order but for a multilayered structure which is cut across the layers).

1. Homogenization in the bulk, the parameter ε_{eff}

We start by writing the wave equation (1) in a slightly different way. Specifically we introduce the vector field $\mathbf{C}$ such as (1) takes the form

$$\mathbf{C} = \nabla E, \quad \mathrm{div}\mathbf{C} + \varepsilon k^2 E = 0, \tag{A1}$$

hence $\mathbf{C}$ is related to the magnetic field. The above formulation is not strictly necessary but it allows for shortcuts in the calculations. The two-scale asymptotic analysis relies on the definition of a rapid scale associated to the periodicity d of the structure, and small means small compared to the wavelength. Without loss of generality, we can choose $k = O(1)$, hence $\eta = d \ll 1$. To this scale is associated a coordinate, in the present one-dimensional case, $\xi = z/\eta$. Next, the solution $(E, \mathbf{C})$ is thought in terms of the expansions

$$\begin{aligned} E &= E^0(\mathbf{x}, \xi) + \eta E^1(\mathbf{x}, \xi) + \eta^2 E^2(\mathbf{x}, \xi) + \cdots, \\ \mathbf{C} &= \mathbf{C}^0(\mathbf{x}, \xi) + \eta \mathbf{C}^1(\mathbf{x}, \xi) + \eta^2 \mathbf{C}^2(\mathbf{x}, \xi) + \cdots, \end{aligned} \quad \text{(A2)}$$

with the $(E^n, \mathbf{C}^n)$ being 1-periodic with respect to ξ [by construction, $\xi \in (-1/2, 1/2)$]. In the bulk of the structure, the differential operator now reads as

$$\nabla \to \nabla_{\mathbf{x}} + \frac{1}{\eta}\frac{\partial}{\partial \xi}\boldsymbol{e}_z. \quad \text{(A3)}$$

Plugging the asymptotic expansions (A2) into (A1) along with (A3), we obtain at the leading order that $\partial_\xi C_z^0 = \partial_\xi E^0 = 0$, from which $E^0(\mathbf{x})$ and $C_z^0(\mathbf{x})$ do not depend on the rapid scale ξ. Then, at each order $n = 0, 1, \ldots$, the system (A1) becomes

$$C_x^n = \frac{\partial E^n}{\partial x}, \quad C_z^n = \frac{\partial E^n}{\partial z} + \frac{\partial E^{n+1}}{\partial \xi}, \quad \text{(A4)}$$

and after averaging over $\xi \in (-1/2, 1/2)$, we obtain

$$\langle C_x^n \rangle(\mathbf{x}) = \frac{\partial \langle E^n \rangle}{\partial x}(\mathbf{x}), \quad \langle C_z^n \rangle(\mathbf{x}) = \frac{\partial \langle E^n \rangle}{\partial z}(\mathbf{x}). \quad \text{(A5)}$$

We also have

$$\frac{\partial C_z^{n+1}}{\partial \xi} + \mathrm{div}_{\mathbf{x}} \mathbf{C}^n + k^2 \varepsilon E^n = 0, \quad \text{(A6)}$$

which after averaging leaves us with

$$\mathrm{div}_{\mathbf{x}} \langle \mathbf{C}^n \rangle + k^2 \langle \varepsilon E^n \rangle = 0. \quad \text{(A7)}$$

From (A5) and (A7), we see that a nontrivial wave equation appears if, in (A7), $\langle \varepsilon E^n \rangle \neq \langle \varepsilon \rangle \langle E^n \rangle$ and we shall see that this happens for $n \geqslant 2$. For the time being, we use (A4) for $n = 0$ to get

$$C_z^0(\mathbf{x}) = \frac{\partial E^0}{\partial z}(\mathbf{x}) + \frac{\partial E^1}{\partial \xi}(\mathbf{x}, \xi), \quad \text{(A8)}$$

which shows that

$$C_z^0(\mathbf{x}) = \frac{\partial E^0}{\partial z}(\mathbf{x}) \text{ and } E^1(\mathbf{x}) \quad \text{(A9)}$$

do not depend on the rapid scale. From (A5) to (A7), the wave equations for $n = 0, 1$ simply involve the average $\langle \varepsilon \rangle$ of $\varepsilon(\xi)$.

To find a nontrivial wave equation, we need E^2, hence we need also C_z^1. With $n = 0$ in (A6), and after integration, we find that

$$\begin{aligned} C_z^1(\mathbf{x}, \xi) &= \hat{\varepsilon}(\xi) k^2 E^0(\mathbf{x}) + \langle C_z^1 \rangle(\mathbf{x}), \\ \text{with } \hat{\varepsilon}(\xi) &= \int_{-1/2}^{\xi} [\langle \varepsilon \rangle - \varepsilon(\chi)] d\chi. \end{aligned} \quad \text{(A10)}$$

To get the above expression, we have used $\mathrm{div}_{\mathbf{x}} \mathbf{C}^0(\mathbf{x}) = -k^2 \langle \varepsilon \rangle E^0(\mathbf{x})$ from (A7). We also used $\langle \hat{\varepsilon} \rangle = 0$ and introduced

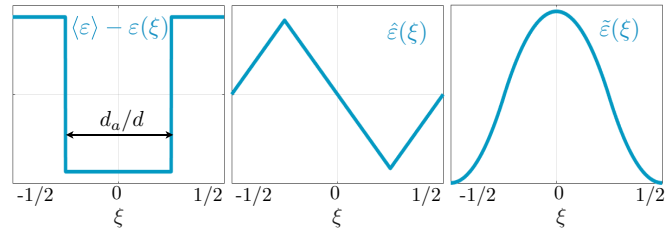

FIG. 13. Functions $\hat{\varepsilon}$ and $\tilde{\varepsilon}$ in (A15) and (A16) for $d_a = d_b = d/2$.

the mean value $\langle C_z^1 \rangle$ of C_z^1. Next, we use C_z^1 in (A4) with $n = 1$, namely,

$$C_z^1(\mathbf{x}, \xi) = \frac{\partial E^1}{\partial z}(\mathbf{x}) + \frac{\partial E^2}{\partial \xi}(\mathbf{x}, \xi), \quad \text{(A11)}$$

from which

$$\begin{aligned} E^2(\mathbf{x}, \xi) &= [\tilde{\varepsilon}(\xi) - \langle \tilde{\varepsilon} \rangle] E^0(\mathbf{x}) + \langle E^2 \rangle(\mathbf{x}), \\ \text{with } \tilde{\varepsilon}(\xi) &= \int_{-1/2}^{\xi} \hat{\varepsilon}(\chi) d\chi, \end{aligned} \quad \text{(A12)}$$

and we used that $\langle C_z^1 \rangle(\mathbf{x}) = \partial_z E^1(\mathbf{x})$ from (A5). In (A7), we have now $\langle \varepsilon E^2 \rangle \neq \langle \varepsilon \rangle \langle E^2 \rangle$, since (A7) reads as

$$\mathrm{div}_{\mathbf{x}} \langle \mathbf{C}^2 \rangle + k^2 [\langle \varepsilon \rangle \langle E^2 \rangle + (\langle \varepsilon \tilde{\varepsilon} \rangle - \langle \varepsilon \rangle \langle \tilde{\varepsilon} \rangle) E^0(\mathbf{x})] = 0, \quad \text{(A13)}$$

while for $n = 0, 1$, we had $\mathrm{div}_{\mathbf{x}} \langle \mathbf{C}^n \rangle + k^2 \langle \varepsilon \rangle \langle E^n \rangle = 0$. It is sufficient to consider the truncation $E \simeq E^0 + \eta E^1 + \eta^2 E^2$ which satisfies an effective wave equation with the permittivity $\varepsilon_{\mathrm{eff}}$,

$$\begin{aligned} &\Delta E + k^2 \varepsilon_{\mathrm{eff}}(k) E = 0, \\ &\text{with } \varepsilon_{\mathrm{eff}}(k) = \langle \varepsilon \rangle + (kd)^2 (\langle \varepsilon \tilde{\varepsilon} \rangle - \langle \varepsilon \rangle \langle \tilde{\varepsilon} \rangle). \end{aligned} \quad \text{(A14)}$$

The functions $\hat{\varepsilon}$ and $\tilde{\varepsilon}$ are defined for $\xi \in (-1/2, 1/2)$ and they read as

$$\frac{\hat{\varepsilon}(\xi)}{(\varepsilon_a - \varepsilon_b)} = \begin{cases} \frac{d_a}{d}(\xi + 1/2), & \xi < -\frac{d_a}{2d}, \\ \frac{d_b}{d}\xi, & |\xi| < \frac{d_a}{2d}, \\ \frac{d_a}{d}(\xi - 1/2), & \xi > \frac{d_a}{2d}, \end{cases} \quad \text{(A15)}$$

$$\frac{\tilde{\varepsilon}(\xi)}{(\varepsilon_a - \varepsilon_b)} = \begin{cases} \frac{d_a}{2d}(\xi + 1/2)^2, & \xi < -\frac{d_a}{2d}, \\ \frac{d_b}{2d}\left(\frac{d_a}{4d} - \xi^2\right), & |\xi| < \frac{d_a}{2d}, \\ \frac{d_a}{2d}(\xi - 1/2)^2, & \xi > \frac{d_a}{2d} \end{cases} \quad \text{(A16)}$$

(see Fig. 13).

Eventually, we get

$$(\langle \varepsilon \tilde{\varepsilon} \rangle - \langle \varepsilon \rangle \langle \tilde{\varepsilon} \rangle) = \frac{1}{12}(\varepsilon_a - \varepsilon_b)^2 \frac{d_a^2 d_b^2}{d^4}, \quad \text{(A17)}$$

hence

$$\varepsilon_{\mathrm{eff}}(k) = \langle \varepsilon \rangle + \frac{k^2}{12}(\varepsilon_a - \varepsilon_b)^2 \frac{d_a^2 d_b^2}{d^2}, \quad \text{(A18)}$$

in agreement with the findings of [13]. The effective wave equations at the orders 1 and 2 ($n = 0, 1$) involve $\langle \varepsilon \rangle$; in the paper they are called HM_1, which coincides with EMA and HM_2. At the third order, HM_3 involves a high-order correction

(A18). We shall now see that HM_2 (whence HM_3) differs from EMA by the transmission conditions at the boundaries of a finite extent structure.

2. Homogenization at a boundary, the parameter $\hat{\varepsilon}$

Here, we shall derive the effective transmission conditions at the dominant nontrivial order, which is the order 2. The fields in the vicinity of one boundary of the multilayered structure are written using new expansions which hold in the vicinity of that boundary only; far from it, they have to coincide with the expansions sought in (A2). Specifically, we consider

$$\begin{aligned} E &= e^0(x,\xi) + \eta e^1(x,\xi) + \cdots, \\ \mathbf{C} &= \mathbf{c}^0(x,\xi) + \eta \mathbf{c}^1(x,\xi) + \cdots. \end{aligned} \tag{A19}$$

The matching with the solution (A2) is written using $z = \eta\xi$ and reexpanding (hence for large ξ and $z \to 0$); we get the matching conditions at the dominant order

$$E^0(x,0^\pm) = \lim_{\xi\to\pm\infty} e^0(x,\xi), \quad \mathbf{C}^0(x,0^\pm) = \lim_{\xi\to\pm\infty} \mathbf{c}^0(x,\xi), \tag{A20}$$

and at the next order

$$E^1(x,0^\pm) = \lim_{\xi\to\pm\infty} \left(e^1(x,\xi) - \xi \frac{\partial E^0}{\partial z}(x,0^\pm) \right), \tag{A21}$$

where we used that at this order $\mathbf{C}^0(\mathbf{x})$ and $E^1(\mathbf{x})$ do not depend on ξ within the layered structure (and obviously not outside). For the matching on $\mathbf{C}^1$, we have to distinguish the two limits $\xi \to \pm\infty$, specifically

$$\begin{aligned} \mathbf{C}^1(x,0^-) &= \lim_{\xi\to-\infty} \left(\mathbf{c}^1(x,\xi) - \xi \frac{\partial \mathbf{C}^0}{\partial z}(x,0^-) \right), \\ \mathbf{C}^1(x,0^+,\xi) &= \lim_{\xi\to+\infty} \left(\mathbf{c}^1(x,\xi) - \xi \frac{\partial \mathbf{C}^0}{\partial z}(x,0^+) \right). \end{aligned} \tag{A22}$$

Near the boundary, the differential operator reads as

$$\boldsymbol{\nabla} \to \frac{\partial}{\partial x}\boldsymbol{e}_x + \frac{1}{\eta}\frac{\partial}{\partial \xi}\boldsymbol{e}_z. \tag{A23}$$

We plug (A19) into (A1) along with (A23); at the dominant order, we obtain $\partial_\xi e^0 = \partial_\xi c_z^0 = 0$, hence $e^0(x)$ and $c_z^0(x)$ do not depend on the rapid scale. Next, the chain rule applies for $n = 0, 1, \ldots,$

$$c_x^n(x,\xi) = \frac{\partial e^n}{\partial x}(x,\xi), \quad c_z^n(x,\xi) = \frac{\partial e^{n+1}}{\partial \xi}(x,\xi), \tag{A24}$$

and

$$\frac{\partial c_z^{n+1}}{\partial \xi} + \frac{\partial c_x^n}{\partial x} + k^2 \varepsilon e^n = 0, \tag{A25}$$

where ε depends on ξ, with $\varepsilon = \varepsilon_{\text{in}}$ for $\xi < 0$ and $\varepsilon = \varepsilon_a, \varepsilon_b$ being periodic for $\xi > 0$. To begin with, we get immediately from (A20) that

$$\begin{aligned} E^0(x,0^\pm) = e^0(x), &\quad \Rightarrow [\![E^0]\!] = 0, \\ C_z^0(x,0^\pm) = c_z^0(x), &\quad \Rightarrow [\![C_z^0]\!] = 0, \end{aligned} \tag{A26}$$

where $[\![f]\!] = f(x,0^+) - f(x,0^-)$. We find at this order the intuitive (and trivial) continuity of the electric field and of the tangential component of the magnetic field. We now move to the next order. From $n = 0$ in (A24), we get that $\partial_\xi e^1 = c_z^0(x)$, hence $e^1(x,\xi) = \xi c_z^0(x) + e^1(x,0) = \xi C_z^0(x) + e^1(x,0)$, and from (A9) and (A26)

$$e^1(x,\xi) = \xi \frac{\partial E^0}{\partial z}(x,0) + e^1(x,0). \tag{A27}$$

It is sufficient to use (A21) to get

$$E^1(x,0^\pm) = e^1(x,0), \quad \Rightarrow [\![E^1]\!] = 0. \tag{A28}$$

The last step consists in integrating (A25) for $n = 0$ between $-\xi$ and ξ, along with $c_x^0(\mathbf{x}) = \partial_x e^0(x) = \partial_x E^0(x,0)$ [from (A24) and (A26)]. We get that

$$c_z^1(x,+\xi) - c_z^1(x,-\xi) + I^-(\xi) + I^+(\xi) = 0, \tag{A29}$$

where we have defined

$$\begin{aligned} I^-(\xi) &= \int_{-\xi}^0 \left(\frac{\partial C_x^0}{\partial x}(x,0) + k^2 \varepsilon_{\text{in}} E^0(x,0) \right) d\chi, \\ I^+(\xi) &= \int_0^\xi \left(\frac{\partial C_x^0}{\partial x}(x,0) + k^2 \varepsilon(\chi) E^0(x,0) \right) d\chi. \end{aligned} \tag{A30}$$

Obviously, we have $I^-(\xi) = -\xi \partial_z C_z^0(x,0)$ since (A1) applies outside the structure, at each order. Next with $E^0(\mathbf{x})$ and $\mathbf{C}^0(\mathbf{x})$ inside the structure, and hence $\text{div}_{\mathbf{x}} \mathbf{C}^0 + k^2 \langle\varepsilon\rangle E^0 = 0$, from (A7), we also have

$$I^+(\xi) = -\xi \frac{\partial C_z^0}{\partial z}(x,0) + k^2 E^0(x,0) \int_0^\xi [\varepsilon(\chi) - \langle\varepsilon\rangle] d\chi.$$

Eventually, using the matching conditions (A22) in (A29) in the limit $\xi \to +\infty$, the terms $\xi \partial_z C_z^0(x,0)$ (linear in ξ) cancel and we get that

$$\begin{aligned} [\![C_z^1]\!] &= k^2 \hat{\varepsilon} E^0(x,0), \\ \text{with} \quad \hat{\varepsilon} &= \int_0^\infty [\langle\varepsilon\rangle - \varepsilon(\chi)] d\chi, \end{aligned} \tag{A31}$$

depends on the arrangement of the layer terminating the structure (Fig. 14). We shall now specify the form of $\hat{\varepsilon}$. Obviously, the integral in (A31) is bounded since the integral of ε over the cell equals its mean. Hence we simply have

$$\hat{\varepsilon} = \int_0^{d_{\text{bl}}/d} [\langle\varepsilon\rangle - \varepsilon(\chi)] d\chi, \tag{A32}$$

where $d_{\text{bl}} < d$ is the distance from the boundary of the structure at $z = 0$ up to the entrance of the first complete unit cell with our convention of the unit cell being centered on the layer of material a. It is easy to see that the expressions given in (5) using $\hat{d}_{\text{in,out}}$ coincide with (A32). Eventually it is worth noting that the result does not depend on which material is used to

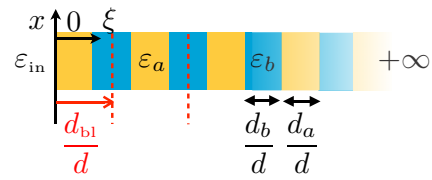

FIG. 14. Boundary layer thickness involved in (A31).

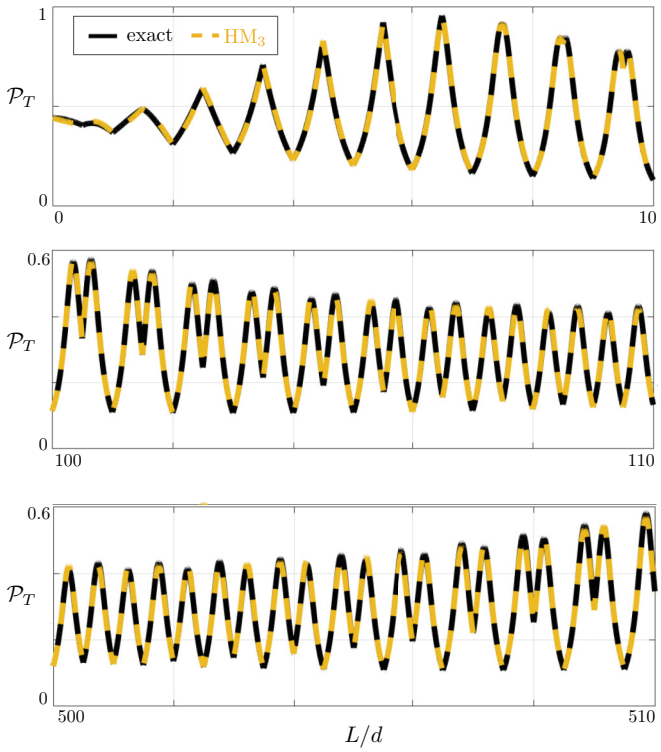

FIG. 15. Transmission as a function of L/d for $kd = 0.5$ and increasing L/d ranges: $L/d \in (0, 10)$, $(100, 110)$, and (500,510). The error in the HM_3 model remains smaller than 1.5%.

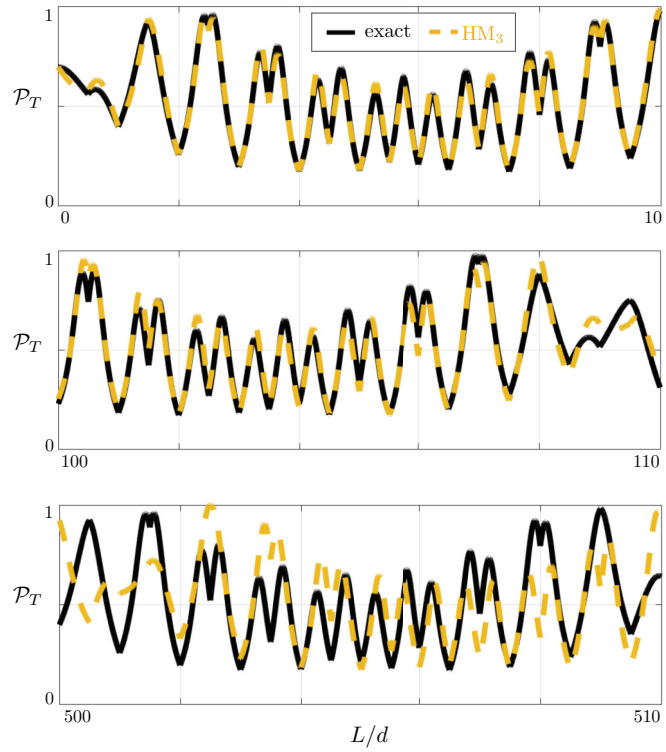

FIG. 16. Same representation as in Fig. 15 for $kd = 1$. The error in the HM_3 model increases for increasing L/d: 3% for $L/d \in (0, 10)$, 10% for $L/d \in (100, 110)$, and 55% for $L/d \in (500, 510)$.

center the unit cell and that the same result can be derived using a noncentered elementary cell.

APPENDIX B: RESULTS IN THE INTERMEDIATE REGIME $kd \sim 1$

Most of the results reported in this study concern the running case $kd \simeq 0.25$ for which the HM_3 prediction is very accurate. As already illustrated in the Fig. 5, the error in the model increases when kd increases and in Fig. 5, with $L/d = 200$, it remains reasonable (less than 10%) up to $kd \sim 1$. In [4], it is said that this intermediate regime where kd becomes close to unity can be of practical interest since it would be less sensitive to disorder and loss. Here, we illustrate the difficulty to reach accurately such regime for a large extent of the structure. To begin with, we have checked for the running case $kd \simeq 0.25$ that the error in the HM_3 model does not exceed 2% up to $L/d = 100\,000$. Next, we report in Fig. 15 the transmission $\mathcal{P}_T$ as a function of L/d for three different ranges $L/d \in (0, 10)$, $(100, 110)$, and (500,510) for $kd = 0.5$, hence slightly higher than our running case. The accuracy in the HM_3 remains very good at about 1% in all cases. Nevertheless, the error increases significantly for very large extent L/d: 10% for $L/d \sim 5000$ and 30% for $L/d \sim 10\,000$ (results are not reported). This is attributable to an increase in the error on the phase accumulation of the wave as already reported for the model HM_2 in Sec. IV A (see Fig. 7).

Eventually, the error becomes visible even for not too large structures for $kd = 1$ (see Fig. 16). At this higher frequency, the increase in the error with the structure extent L/d follows the same tendency as for $kd = 0.5$ but starting with a higher error of 3% for $L/d \in (0, 10)$, it becomes significant for larger extent: 10% in (100,110) and 55% in (500, 510).

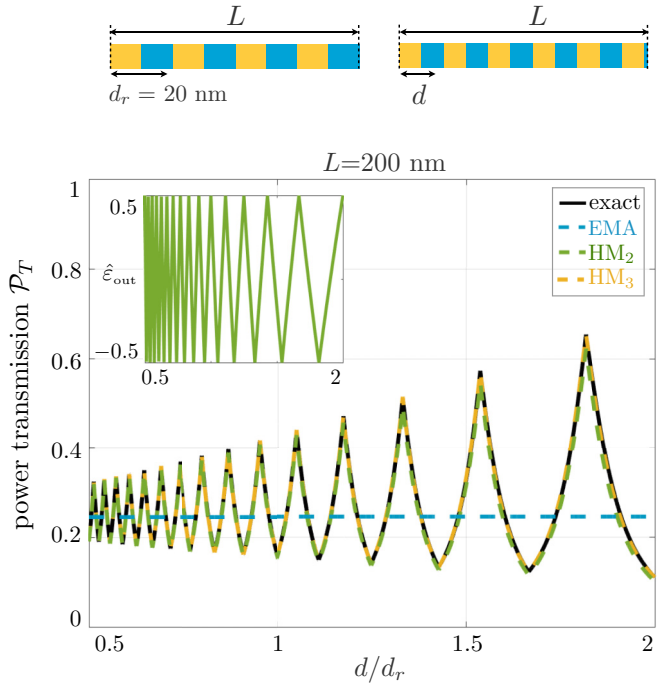

FIG. 17. Transmission dictated by the boundary layer effects ($L = 200$ nm, $\varepsilon_{\text{out}} = \varepsilon_{\text{eff}}$, $\theta = 60^\circ$); the layers have a small variability in thickness $d \in (d_r/2, 2d_r)$ with $d_r = 20$ nm. The inset shows the $\hat{\varepsilon}_{\text{out}}$ against d/d_r.

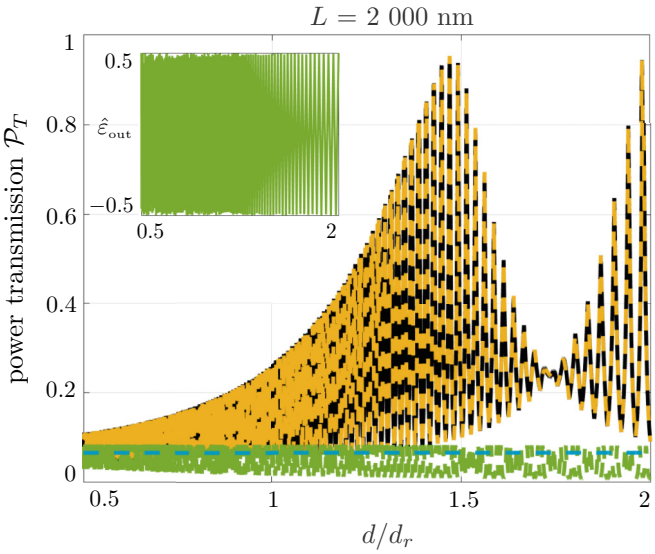

FIG. 18. Same representation as in Fig. 17 for $L = 100d_r$.

From what we have seen, it is difficult to anticipate up to which frequency a homogenized model will be accurate (only the convergence rate against kd can be anticipated). In the present case, the slow phase accumulation during wave propagation produces a significant error. Specifically, for the configuration considered in [4], we found that the error is reasonable in the intermediate regime $kd \sim 0.5$ for structures whose extent does not exceed about $1000d$ and $kd \sim 1$ for structures whose extent does not exceed about $100d$.

APPENDIX C: INFLUENCE OF THE LAYER THICKNESS

In this Appendix, we provide additional results on the unexpected scattering properties of multilayered structure and the accuracy of HM_3 to capture it. Here we shall interrogate the influence of the layer thickness; doing so, we modify both the boundary layer effects and the effective permittivity in the bulk.

We first consider a structure of relatively small extent $L = 200$ nm, hence $N = 20$ layers in the reference case where $d = d_r = 20$ nm, and we introduce a small variability in the layer thickness with $d \in (d_r/2, 2d_r)$. Within the same extent L, we kept a complete layer at the entrance resulting in a constant value of $\hat{\varepsilon}_{\text{in}}$ while $\hat{\varepsilon}_{\text{out}}$ varies with d. The resulting variations of the power transmission $\mathcal{P}_T$ are reported in Fig. 17. For such a small extent, the phase accumulation during wave propagation is negligible, hence the relatively large variations are attributable to the boundary layer effects only (the variations of $\hat{\varepsilon}_{\text{out}}$ are reported in the inset); this is confirmed by the ability of HM_2 to describe them. It is worth noting that the constant value predicted by EMA (dotted blue line) corresponds to the limit of vanishing d.

We now consider a larger structure $L = 2000$ nm (Fig. 18). In this case, cooperation between boundary layer effects and the phase accumulation produces a more complex spectrum, with rapid variations dictated by d through $\hat{\varepsilon}_{\text{out}}$ and smooth variations due to phase accumulation since αL is of the order unity; for $\theta = \theta_c$, $\alpha = k^2 d/\sqrt{12}$ reaches π for $d/d_r \sim 1.7$. This phase accumulation is not accounted for properly in EMA and HM_2 which fails in predicting the large-scale variations (in comparison HM_3 has an overall accuracy of 0.5%).

[1] J. Schilling, Phys. Rev. E **74**, 046618 (2006).
[2] A. V. Chebykin, A. A. Orlov, A. V. Vozianova, S. I. Maslovski, Y. S. Kivshar, and P. A. Belov, Phys. Rev. B **84**, 115438 (2011).
[3] J. Elser, V. A. Podolskiy, I. Salakhutdinov, and I. Avrutsky, Appl. Phys. Lett. **90**, 191109 (2007).
[4] H. Herzig Sheinfux, I. Kaminer, Y. Plotnik, G. Bartal, and M. Segev, Phys. Rev. Lett. **113**, 243901 (2014).
[5] A. Andryieuski, A. V. Lavrinenko, and S. V. Zhukovsky, Nanotechnology **26**, 184001 (2015).
[6] S. V. Zhukovsky, A. Andryieuski, O. Takayama, E. Shkondin, R. Malureanu, F. Jensen, and A. V. Lavrinenko, Phys. Rev. Lett. **115**, 177402 (2015).
[7] H. H. Sheinfux, Y. Lumer, G. Ankonina, A. Z. Genack, G. Bartal, and M. Segev, Science **356**, 953 (2017).
[8] H. H. Sheinfux, I. Kaminer, A. Z. Genack, and M. Segev, Nat. Commun. **7**, 12927 (2016).
[9] A. V. Chebykin, A. A. Orlov, C. R. Simovski, Y. S. Kivshar, and P. A. Belov, Phys. Rev. B **86**, 115420 (2012).
[10] M. G. Silveirinha, Phys. Rev. B **75**, 115104 (2007).
[11] V. Popov, A. V. Lavrinenko, and A. Novitsky, Phys. Rev. B **94**, 085428 (2016).
[12] V. Popov, A. V. Lavrinenko, and A. Novitsky, Phys. Rev. B **97**, 125428 (2018).
[13] X. Lei, L. Mao, Y. Lu, and P. Wang, Phys. Rev. B **96**, 035439 (2017).
[14] C. Rizza and A. Ciattoni, Phys. Rev. Lett. **110**, 143901 (2013).
[15] C. Rizza, E. Palange, and A. Ciattoni, Photonics Res. **2**, 121 (2014).
[16] C. Rizza, V. Galdi, and A. Ciattoni, Phys. Rev. B **96**, 081113 (2017).
[17] J.-J. Marigo and A. Maurel, SIAM J. Appl. Math. **77**, 721 (2017).
[18] K. Pham, A. Maurel, and J.-J. Marigo, J. Mech. Phys. Solids **106**, 80 (2017).
[19] L. Schwan, O. Umnova, C. Boutin, and J.-P. Groby, J. Appl. Phys. **123**, 091712 (2018).
[20] P. A. Belov, R. Marques, S. I. Maslovski, I. S. Nefedov, M. Silveirinha, C. R. Simovski, and S. A. Tretyakov, Phys. Rev. B **67**, 113103 (2003).
[21] C. R. Simovski, J. Opt. **13**, 013001 (2010).
[22] D. T. Le, Modèle d'endommagement à gradient: Approche par homogénéisation, Doctoral dissertation, Université Pierre et Marie Curie-Paris VI, 2015.
[23] A. Abdulle and T. N. Pouchon, Effective models for long time wave propagation in locally periodic media, No. EPFL-article-231084 (2017).